NIH Public Access
Author Manuscript
Biochemistry. Author manuscript; available in PMC 2012 May 17.

Published in final edited form as:
Biochemistry. 2011 May 17; 50(19): 3903–3912. doi:10.1021/bi200083d.

Structural Basis of the RNase H1 Activity on Stereo Regular Borano Phosphonate DNA/RNA Hybrids

Christopher N Johnson[1], **Alexander M. Spring**[1], **Barbara R. Shaw**[3], and **Markus W. Germann**[1,2]

[1] Department of Chemistry, Georgia State University

[2] Department of Biology and the Neuroscience Institute, Georgia State University

[3] Department of Chemistry, Duke University

Abstract

Numerous DNA chemistries have been explored to improve oligodeoxynucleotide (ODN) based RNA targeting. The majority of the modifications render the ODN/RNA target insensitive to RNase H1. Borano phosphonate ODN's are among the few modifications that are tolerated by RNase H1. To understand the effect of the stereochemistry of the BH_3 modification on the nucleic acid structure and RNase H1 enzyme activity we have investigated two DNA/RNA hybrids containing either a R_P or S_P BH_3 modification by NMR spectroscopy. T_M studies show that the stability of either R_P or S_P modified DNA/RNA hybrids are essentially identical (313.8 K) and similar to an unmodified control (312.9 K). The similarity is also reflected in the imino proton spectra. In order to characterize such similar structures, a large number of NMR restraints (including dipolar couplings and backbone torsion angles) were used to determine structural features important for RNase H1 activity. The final NMR structures exhibit excellent agreement with the data (total R^X values < 6.0) with helical properties between those of an A and B helix. Subtle backbone variations are observed in the DNA near the modification, while the RNA strands are relatively unperturbed. In case of the S_P modification, for which more perturbations are recorded, a slightly narrower minor groove is also obtained. Unique NOE base contacts localize the S_P -BH_3 group in the major groove while the R_P -BH_3 group points away from the DNA. However, this creates a potential clash of the R_P -BH_3 groups with important RNase H1 residues in a complex while the S_P -BH_3 groups could be tolerated. We therefore predict that based on our NMR structures a fully R_P BH_3 DNA/RNA hybrid would not be a substrate for RNase H1.

With the advent of antisense technologies over a decade ago, a number of approaches have been developed for the regulation of gene expression through inhibition via the introduction of a short, RNA complementary DNA oligonucleotide (ODN) and the potential ribonuclease H (RNase H1) mediated degradation of the RNA strand (1, 2, 3). The challenges with this technique range from increasing the inherently low lipophilicity of the ODN to its

Phone: 404-413-5561, Fax: 404-413-5505, mwg@gsu.edu.

Coordinates and NMR derived restraints have been deposited in the Protein Data Bank (R_p hybrid 21ar, S_p hybrid 21b4) and Biological Magnetic Resonance Bank (17535)

Supplemental Information:
The following supplemental information is available free of charge via the internet at http://pubs.acs.org: Tables of ^{1}H, ^{11}B, ^{13}C, and ^{31}P NMR resonance assignments for the Rp, Sp, and control hybrids, NOESY base H6/H8 to H1′ pathways, ε torsion angles for Rp and Sp, H1′–H2′1 and H1′–H2′2 aligned low flip angle COSY spectra, plots of selected helical parameters of the final Rp and Sp hybrid structures, summary sugar puckering plots for the Rp and Sp hybrids, description of the BH_3 Amber force-field modification methodology, and Amber 9.0 and REDCAT back calculated RDC values and plots as compared to experimentally determined RDC values.

NIH-PA Author Manuscript
NIH-PA Author Manuscript
NIH-PA Author Manuscript

NIH-PA Author Manuscript

NIH-PA Author Manuscript

NIH-PA Author Manuscript

degradation by nucleases. Many DNA modifications have been developed in an attempt to circumvent these undesirable properties, which have unfortunately been found to create their own sets of issues; one of the biggest being the inability to activate RNase H1. To overcome this, many types of modifications have been explored (methylphosphonates, 2′ modifications, locked nucleic acids, peptide nucleic acids, and morpholino substitutions among others). While the target affinity has been greatly increased for some of these modifications (PNA and morpholino substitutions, for instance) the resulting hybrids are not substrates for RNase H1 (4, 5, 6).

Although binding of an ODN to the mRNA may still silence a gene, RNase H1 activity of an ODN is deemed desirable because it allows a single ODN to mediate the destruction of multiple RNA targets (7). A recent structure of the human RNase H1 in complex with a DNA/RNA duplex has provided insight into the binding process and substrate conformations involved in binding (8). This has sparked a renewed interest in RNase H1 activity and substrate specificity.

Only a few ODN modifications are able to preserve RNase H1 activity (i.e. phosphorothioate, phosphorodithioate, arabinonucleic acids, and boranophosphates) (9, 10, 11) (12). The phosphorothioate diester linkage maintains a pseudo-isoelectronic and isosteric character with a phosphodiester linkage, is relatively easy to synthesis and maintains canonical sugar and base moieties, but it creates a chiral center at the phosphate linkage. This modification has been found to permit RNase H1 activity yet is resistant to nuclease degradation, but suffers from toxicity at higher concentrations, non specific interactions with many cellular components and poor RNA binding (6). Most other backbone modifications, including methylphosphonates, are not substrates for RNase H1 (3).

Aside from the phosphorothioate, the borano phosphate modification (insertion of a BH_3 group in place of a non-linking oxygen) has also been shown to maintain RNase H1 activity. Further, it increases lipophilicity while maintaining binding to the targeted mRNA and exhibits a relatively low toxicity. The borano modification has an isosteric relationship with the methylphosphonate group, but maintains a negative charge and is isoelectronic with the oxygen of the phosphodiester group. Coupled with a minimal toxicity, the borano phosphate diester linkage continues to show promise (13,14, 15).

Similar to the phosphorothioate modification, the introduction of the borano group creates a chiral center at the phosphorus (Figure 1). Stereoregular studies of phosphorothioate linkages revealed that RNase H1 activity is modulated based on the stereochemistry with the R_P isomer (the sulfur pointing towards the helix) retaining RNase H1 activity while for the S_P isomer the enzymatic activity is reduced as compared to the natural phosphodiester linkage (16). Previous studies have shown that a fully S_p stereo-specifically modified borano phosphate (borano group pointing towards the helix) containing oligonucleotide retains RNase H1 activity (15). * To date, R_P ODN's containing a fully modified backbone have not been studied because such ODN's cannot be enzymatically generated and have to be chemically synthesized (15, 17).

Here, we report the high resolution NMR solution structures of two DNA/RNA duplex nonamers containing either a single S_P or R_P borano phosphate modification. This represents the first detailed fine structural analysis of stereo-regular borano phosphate modifications. In conjunction with a recently solved crystal structure of human RNase H1 in complex with a

*The stereochemistry of phosphorothioate R_P is equivalent to borano phosphate S_P due to the lower priority of boron as compared to oxygen and sulfur.

NIH-PA Author Manuscript

NIH-PA Author Manuscript

NIH-PA Author Manuscript

DNA/RNA duplex, we provide a rational for why the S_P hybrid is a substrate for the enzyme while we predict that the R_P hybrid is not (8).

Materials and Methods

The DNA oligonucleotides were synthesized containing a single stereo specific modification (replacement of a non-bridging phosphodiester backbone oxygen with BH_3 group) at T_5-P-G_6 as previously described (18, 19). Oligonucleotides were purified and characterized by anion exchange, reverse phase chromatography, and mass spectroscopy. The stereochemistry of the borano phosphonate linkages were confirmed by snake venom digestion as described previously (20). DNA/RNA duplexes were prepared using extinction coefficients derived from the sum of mononucleotides (absorbance at 260 nm, 80°C, in 10 mM sodium phosphate) as described previously (21). For all NMR experiments, samples were prepared in: 10 mM sodium phosphate, 50 mM NaCl, and 0.1 mM Ethylenediaminetetraacetic acid (EDTA). Water samples (90/10 % H_2O/D_2O) were 80 μM DNA/RNA duplex with a pH of 6.2, and samples in D_2O were ~1.0 mM DNA/RNA duplex with a pH* of 6.6. For residual dipolar coupling experiments, pf1 bacterial phage was purchased from Asla and prepared as previously described (22). Prepared pf1 (~ 53 mg/ml) was added to NMR samples in appropriate aliquots and a deuterium splitting of 20.8 Hz was observed at 298 K.

Melting Temperature Studies

T_M values were derived from a six parameter fit of UV melting curves for a series of concentrations ranging from 5 μM–50 μM duplex. The enthalpy was obtained from the concentration dependence of the T_M values and entropy. T_M (30 μM C_T) and ΔS were calculated using an equation for the biomolecular association of non-self complementary strands as described previously (21).

NMR Spectroscopy

NMR experiments were performed on Bruker AMX 600 and Avance 600 spectrometers, using a 5mm IDTG-600 triple resonance (Nalorac Corp) and broadband inverse Bruker probe heads. Acquisition and processing parameters are similar to those described in earlier studies (21) with the following variables; for experiments in D_2O, NOESY spectra were collected with mixing times of 50 ms, 150 ms, and 250 ms with an 8 sec delay to ensure complete relaxation, ^1H - ^{31}P correlation (HPCOR) (23) spectra were strip transformed and processed with a shifted sine bell multiplication in both dimensions (SSB = 2). For water experiments, a 1-1 jump and return and a 1-1 jump and return NOESY with a 150 ms mixing time were used with a 0.3 sec delay at 298 K and 280 K. Assignment and integration of 2D spectra were done using SPARKY 3.33 UCSF (24). ^1H and ^{31}P were referenced to internal DSS and external 85% H_3PO_4 (capillary in D_2O). Constant time NOESY (CT NOESY) experiments were collected using a 12 ms REBURP pulse to select the sugar H3′ region (25). Boron spectra were collected for ^{11}B, (^{11}B: spin 3/2, 80.42% natural abundance, compared to ^{10}B: spin 3, 19.58% natural abundance) and were referenced to an external standard (0.80 M borate from tris borate EDTA, 298 K, pH = 8.36). Heteronuclear f2 coupled ^{13}C - ^1H HSQC spectra were recorded for sugars (^{13}C range 65–105 ppm) and bases (^{13}C range 125–175 ppm) in the presence and absence of pf1 phage.

Starting Structures

Initial DNA/RNA hybrids were constructed using Amber 9.0's NUCGEN (26). Using Xleap with a modified parm99 force-field (added BH_3 group), a non-bridging oxygen on the DNA backbone between bases T_5 and G_6 was replaced by a borano (BH_3) group to yield two hybrids with a single R_P or S_P configuration. Sodium ions were added to neutralize the

NIH-PA Author Manuscript

NIH-PA Author Manuscript

NIH-PA Author Manuscript

phosphodiester backbone and the systems were solvated with at least 8.0 Å from the edge of the solute to the edge of a box with ~ 3200 TIP3P water molecules.

Briefly, the BH_3 force field modification was constructed as follows; for the B-P distance the empirically determined value of 1.91Å was used (27). This distance was found to be reproducible using HF 6-31G* energy minimizations. Atomic point charges were derived via an iterative process using Gaussian 03, the AMBER 9.0 RESP module, and the RED program (28, 26, 29a,b). The R_P and S_P conformers utilize the same parameters with the exception of the BH_3 group placement. For more details on the derivation of the BH_3 group parameters see Supplemental Information 6.

Structure Determination

^{1}H resonances were assigned via 2D ^{1}H NOESY pathways with the assistance of TOCSY and COSY spectra. ^{31}P resonances were assigned based on HPCORR correlation experiments. NOESY cross peak volumes were integrated in SPARKY using a Gaussian or Sum Over Box method. A percentage error was manually assigned based upon the fit residual & visual inspection of a projected cross slice overlaid with the integral trace. For unresolved peaks, a Sum Over Box integration method was used and a higher percentage error was assigned. Peak volumes for base H8 protons were manually scaled to correct for exchange with the deuterated solvent based on the integration of a 1D ^{1}H spectrum collected with an 8 sec delay. Quantitative distance restraints were derived using an iterative RANDMARDI procedure using COMRA, MARDIGRAS (30, 31) and AMBER 9.0 cycles, as described previously (21). R^x values were calculated in CORMA using correlation times (τ_C) 2.5 ns, 3.0 ns, 3.5 ns and 4.0 ns for base and sugar protons. The overall lowest values were obtained for τ_C = 3.5 ns. DNA sugar pucker and pseudorotation angles were assessed using a graphical method from the Altona lab (32). $^3J_{H1'-H2'1}$, $^3J_{H1'-H2'2}$, $^3J_{H1'-H3'}$, Σ H1′ and Σ H3′ were measured from ^{31}P decoupled low flip angle and DQF COSY experiments. Pseudorotation angles were derived for the dominant form of each deoxyribose and converted to torsion angle NMR restraints using the PUCKER script from Amber 9.0. Due to extensive overlap at multiple temperatures, the sugar pucker at the core of the S_P hybrid (G_4, T_5, and G_6) and R_P hybrid (G_3, G_6) were estimated based upon ^{13}C1′ chemical shifts in conjunction with the analysis of the glycosidic torsion angle and base H6/H8 to sugar H3′ NOESY cross peak intensities.

Backbone ε torsion restraints were derived based on the ratio of peak heights from CT NOESY experiments (^{31}P coupled vs. decoupled) as described in (25). Broad backbone torsion angle restrains for α, β, γ, and ζ, were generated for nucleotides having standard ^{31}P chemical shifts using values from Blackburn *et. al.* (33, 34).

Residual Dipolar Coupling (RDC) restraints were derived from $^1J^{13}_{C-}{}^1_H$ values measured in the f2 dimension in presence and absence of pf1 ($\Delta^1J^{13}_{C-}{}^1_H$ values ranged from −14 Hz, +15 Hz). All RDC restraints were implemented at the end of the structure generation process by initially minimizing the alignment tensor of the rigid hybrid, followed by fully restrained minimization (rEM) of the whole system. Following RDC implementation, each system (R_P and S_P hybrid) underwent a 6.0 ns fully restrained MD simulation with RDC alignment at 300 K. Snapshots were recorded 1/ps for the final 10 ps and individually minimized to all restraints yielding a final bundle of structures. Final structures were selected based on Amber energies, restraint violations, and residual dipolar coupling violations. RMSD was calculated for heavy atoms using VMD 1.9. Structural features and helicoidal parameters were measured using CURVES 5.1 (35, 36).

NIH-PA Author Manuscript

NIH-PA Author Manuscript

NIH-PA Author Manuscript

Results

Thermodynamic Stability

UV melting curves of the modified DNA/RNA hybrids were unaffected by the orientation of the BH_3 group. Thermodynamic properties ΔG and T_M were the same for the R_P and S_P hybrids and were comparable to an unmodified DNA/RNA hybrid at similar conditions (21) (Table 1). This indicates that neither orientation nor presence of a single BH_3 modification impacts the thermodynamic stability.

Base Stacking and Orientation

Chemical shifts (^1H, ^{13}C, ^{31}P, and ^{11}B) for the R_P hybrid, S_P hybrid, and unmodified control are listed in Supporting Information 4.

Comparing the ^1H chemical shifts to an unmodified DNA/RNA hybrid, both modified hybrids have small differences at the center of the duplex, while the ends remain indifferent to the presence of the BH_3 modification as would be expected (Figure 2). Chemical shifts of the R_p more closely resembled the unmodified control, with only a few variations for the DNA sugars surrounding the modification ($\Delta \Sigma$ sugar $^1H's$ |, T_5 0.32 ppm, G_6 0.23 ppm) (Figure 2). The S_p hybrid displays larger and more extensive chemical shifts differences in the sugars ($\Delta \Sigma$ |sugar $^1H's$ |, G_4 0.50 ppm, T_5 0.54 ppm,) and bases (T_5 H6 0.16 ppm) at the 5′ side of the DNA modification, with moderate differences extending into the RNA strand (standard deviations were < 0.004 ppm) (Figure 2).

Complete base H8/H6 to sugar H1′ NOESY pathways for both modified samples support normal base stacking (also supported by thermodynamic data) and are consistent with a right handed duplex (37) (Supporting Information 1 a,b). NOESY cross peaks with unusual intensities or exchange peaks were not observed among the base or sugar protons demonstrating that the R_P and S_P modifications do not grossly perturb or induce multiple conformations to the duplex.

Base Pairing

The presence of an imino proton peak generally results from a stable base pair formation. At 280 K we observe all nine imino proton peaks for both modified duplexes establishing that the BH_3 modification does not disrupt base pairing (Figure 2). Comparing the imino proton chemical shifts to the control hybrid, the R_P hybrid is again similar to the unmodified control while the S_p modification shows a difference at the 5′ side of the DNA (Figure 2, Figure 3).

Backbone

Unusual phosphorus chemical shifts are a likely indicator for abnormal torsion angles in the nucleic acid helical phosphodiester backbone that may perturb the helical rise, roll, or twist of a duplex (38). Comparing the phosphorus chemical shifts of a control hybrid with the R_P and S_P modified hybrids, again the R_p hybrid displays less variation from the control (Figure 2). Similar to the trends of the ^1H chemical shifts, the S_P hybrid phosphorus chemical shifts are more perturbed, predominantly on the DNA 5′ side of the modification with effects extending into the RNA strand (c_{15}-P-c_{16}) (Figure 2). As expected, T_5-P-G_6 is shifted downfield for both modified hybrids (R_p 94.00 ppm, S_P 95.38 ppm) due to the BH_3 modification (39) (Figure 4).

The ^{11}B spectrum shows a broad peak (coupled to ^{31}P and ^1H) for both modified hybrids (R_P −41.43 ppm, S_P −42.11 ppm) (Figure 5). Proton decoupling of the boron spectrum reveals the boron phosphorus coupling ($^1J_{BP}$ ~133 Hz) (Figure 5).

NIH-PA Author Manuscript

NIH-PA Author Manuscript

NIH-PA Author Manuscript

Similarly, in the ^{1}H spectrum a broad peak is observed for each hybrid from the BH_3 methyl group (R_P 0.33 ppm, S_P 0.42 ppm) (Figure 5). Decoupling ^{11}B sharpens this peak to a doublet ($^{2}J_{HP}$ = 21.4 Hz) which facilitates the detection of NOE's from the BH_3 group to nearby sugars and bases (Figure 6). The R_P hybrid displays strong NOESY cross peaks to the surrounding sugars while for the S_P hybrid neighboring base contacts are also detected (Figure 6).

The phosphodiester backbone torsion angle ε was determined for the DNA linkages using a CT NOESY experiment (25). All DNA ε torsion angles were within a standard trans range (−158° to −188°) consistent with B DNA helical values (34) (Supporting Information 2). The ε torsion angles that could be determined for the RNA (−145° to −158°) were in line with A type helical parameters.

Pseudorotation Analysis

DNA sugar conformation (expressed as fraction south, f_S) was determined from coupling constants $^{3}J_{H1'-H2'1}$, $^{3}J_{H1'-H2'2}$, $^{3}J_{H1'-H3'}$, Σ H1′ and Σ H3′ (32). Due to extensive overlap across a range of temperatures, the f_S at the core of the S_P hybrid (G_4, T_5, and G_6) and G_3, G_6 of the R_P hybrid, was estimated based on $^{13}C1'$ chemical shifts in conjunction with analysis of the glycosidic torsion angle and base H6/H8 to sugar H3′ NOESY cross peak intensities (Supporting Information 6b,c).

The trends in f_S for residues not flanking the modification mimic the unmodified control hybrid (Supporting Information 3 and 6a). The R_P hybrid more closely resembles the unmodified control with moderate changes in the fraction south for G_4 and T_5. The S_P hybrid likely exhibits larger variations (lower f_S) from the control at G_4 and T_5 based upon the elevated $^{13}C1'$ chemical shifts and more intense base–H3′ cross peaks. (Supporting Information 6a,c).

NMR Structure Determination

Both modified hybrid structures are highly restrained (~23 restraints/nucleotide) and exhibit excellent agreement between theoretical and experimental data as evidenced from the low CORMA total R^x values that are less than 6%. The final ensemble of 10 structures, sampled at the end of a 6.0 ns rMD, yield a heavy atom RMSD below 0.35 Å (Table 2, Figure 7). Amber distance violations were higher for the R_P hybrid (103.9 kcal/mol) compared to the S_P hybrid (51.5 kcal/mol), this is largely due to a narrower average well width (0.47 Å vs. 0.64 Å) for the quantitative restraints (Table 2). For both structures the highest distance penalty was observed for A_1H8-A_1H1' (~8 kcal/mol) and is likely a result of mobility in the adenosine base due to its location at the end of the duplex. All other distance penalties were less than 5.0 kcal/mol (Table 2). Flat angle and torsion angle penalties were negligible (total < 3.5 kcal/mol) for both structures. Residual dipolar coupling alignment data was fit to both structures with excellent agreement, yielding a total alignment constraint of < 7.5 kcal/mol (Table 2).

Analysis of the NMR Structures

The single BH_3 DNA backbone modification does not grossly perturb either DNA/RNA hybrid as compared to an unmodified DNA/RNA hybrid (40) (Figure 8, Supporting Information 5). Both modified hybrids are fully base paired, right handed, and exhibit a majority of A- type helical properties, similar to previously published DNA/RNA hybrid structures (40) (21). All glycosidic bonds are in the anti conformation and the helical parameters X-displacement, Y displacement, incline, rise, and twist, are intermediate of canonical A and B helices with an emphasis towards the A helical form (Table 3, Supplemental Information 5).

NIH-PA Author Manuscript

NIH-PA Author Manuscript

NIH-PA Author Manuscript

Aligning the heavy atoms of the two hybrids (excluding the BH_3 group) yields an RMSD of 1.19 Å. Figure 8. Qualitative distance restraints involving the BH_3 group point the S_P BH_3 modification into the major groove while the R_P group extends out from DNA backbone (Figure 8a). On the 5′ side of the modification (bases G_3, G_4, and T_5) the two structures exhibit small differences in the base opening, buckle, and tilt, resulting in a slight bulge in the S_P DNA backbone (Figure 8b). This is also supported by trends in differences of the ^1H, ^{13}C and ^{31}P chemical shifts and the fact that the only substantial difference in imino ^1H shift between the two hybrids occurs at T_5. The slight backbone deviation in the S_P hybrid narrows the apparent minor groove altering $c_{16}C1'$ chemical shift by 0.8 ppm (Figure 8b). The ends of the duplex as well as the RNA strands (RMSD of RNA 0.82 Å) are nearly identical between both modified hybrids and remain indifferent to the BH_3 modification. (Figure 8a,b).

Discussion

RNase H1, an enzyme found in bacteria and humans, degrades the RNA strand of a DNA/RNA hybrid duplex. Earlier studies attempted to utilize the enzyme as a means of regulating protein expression (41, 42). It is now known that RNase H exists in two types (H1 and H2). While RNase H1 may have potential use in gene regulation, unintentional interference with RNase H2 can result in neurological disorders such as Aicardi-Goutieres syndrome (43).

Previous work from our laboratories has shown that a polynucleotide (15mer) DNA/RNA hybrid containing fully stereo specific (S_p) BH_3 modified DNA backbone linkages maintains RNase H1 activity (14). Here we provide a rational why the BH_3 stereo specific S_P hybrid is a substrate for RNase H1. Two DNA/RNA hybrid NMR solution structures were determined utilizing a large number of restraints (Figure 1). This coupled with the low R^X values permits an analysis of possible fine structural details and subtle features that may impact interactions with the enzyme. The single BH_3 modification is minimally invasive to the overall structure of the DNA/RNA hybrid, with only a slight bulge detected at the 5′ side of the S_P modification. Given the high degree of similarity between the structures and an unmodified control, the question arises if they differ in their interaction with RNase H1.

RNase H1 contains two conserved nucleic acid binding domains. The DNA basic protrusion assists in the initial binding of the substrate duplex. The phosphate binding pocket binds the substrate, forms contacts along the DNA backbone and positions the duplex in order to place the targeted RNA in the proper location for cleavage. RNase H1 is able to bind both DNA/RNA and RNA/RNA duplexes, however RNA cleavage only occurs for the DNA/RNA hybrid. The flexibility of the DNA strand permits a snug fit into the phosphate binding pocket which enables the proper placement of the adjacent RNA target strand in the cleavage site. However, in an RNA/RNA duplex, the lack of flexibility and the presence of hydroxyl groups hamper proper binding to the phosphate binding pocket which displaces the target strand from the cleavage site, resulting in a loss of RNA degradation activity (8).

As evidenced from our NMR structures, either single modification is well tolerated in a duplex and results in modest perturbations, therefore a fully stereo specific modified DNA backbone should not grossly distort a DNA/RNA hybrid. In this context, our structural NMR results provide a rationale for the observed enzyme activity of the S_P BH_3 modified DNA/RNA hybrid (14). The orientation of the BH_3 plays a critical role in avoiding steric clashes with essential RNase H1 contacts. In the S_P hybrid the BH_3 group points away from the enzyme surface into the major groove allowing the DNA strand access to the RNase H1 phosphate binding pocket (Figure 9). Examination of our NMR structures together with the crystal complex (8) predicts that the enzyme can accommodate the S_P orientation of a fully BH_3 modified DNA backbone and maintain RNA cleavage activity. This is in line with

NIH-PA Author Manuscript

NIH-PA Author Manuscript

NIH-PA Author Manuscript

experimental data. In the case of the R_P hybrid, the BH_3 modification would obstruct the required snug fit of the DNA into the enzyme's phosphate binding pocket (Figure 9). Additionally, changes in the local charge distribution compared to a regular phosphodiester linkage may also play a role in modulating the enzyme binding affinity. Taken together these results indicate that the R_P BH_3 group is likely to impede access to essential enzyme binding contacts, thus resulting in loss of RNase H1 RNA cleavage activity (Figure 9).

Supplementary Material

Refer to Web version on PubMed Central for supplementary material.

Acknowledgments

CNJ and AMS were supported by the Brain and Behavior and Molecular Basis of Disease program at GSU respectively.

This work was supported by grants from the NIH AI/GM47459 and the Georgia Cancer Coalition.

Abbreviations

ODN	oligodeoxynucleotide
RNase H1	ribonuclease H
HPCOR	^{1}H–^{31}P correlation
CT NOESY	constant time NOESY
rEM	restrained minimization

References

1. McClorey G, Moulton HM, Iversen PL, Fletcher S, Wilton SD. Antisense oligonucleotide-induced exon skipping restores dystrophin expression in vitro in a canine model of DMD. Gene Therapy. 2006; 13:1373–1381. [PubMed: 16724091]
2. Nicholas MD, MCKAY R. Inhibition of protein kinase C-a expression in mice after systemic administration of phosphorothioate antisense oligodeoxynucleotides. Proc Natl Acad Sci. 1994; 91:11762–11766. [PubMed: 7972137]
3. Stein CA. Is irrelevant cleavage the price of antisense efficacy? Pharmacology & Therapeutics. 2000; 85:231–236. [PubMed: 10739877]
4. Egli M, Minasov G, Tereshko V, Pallan PS, Teplova M, Inamati GB, Lesnik EA, Owens SR, Ross BS, Prakash TP, Manoharan M. Probing the Influence of Stereoelectronic Effects on the Biophysical Properties of Oligonucleotides: Comprehensive Analysis of the RNA Affinity, Nuclease Resistance, and Crystal Structure of Ten 2′-*O*-Ribonucleic Acid Modifications. Biochem. 2005; 44:9045–9057. [PubMed: 15966728]
5. Spurgers KB, Sharkey CM, Warfield KL, Bavari S. Oligonucleotide antiviral therapeutics: Antisense and RNA interference for highly pathogenic RNA viruses. Antiviral Research. 2008; 78:26–36. [PubMed: 18258313]
6. Kurreck J. Anitsense Tehnologies. Eur J Biochem. 2003; 270:1628–1644. [PubMed: 12694176]
7. Aramini, JM.; Van de Sande, JH.; Markus, W.; Germann, MW. Structure and Stability of DNA Containing Inverted Anomeric Centers and Polarity Reversals. In: Leontis, Neocles B.; Lucia, John Santal, Jr, editors. Molecular Modeling of Nucleic Acids; ACS Symposium Series; Washington DC: American Chemical Society; 1998. p. 92-105.
8. Nowotny M, Gaidamakov SA, Ghirlando R, Cerritelli SM, Crouch RJ, Yang W. Structure of Human RNase H1 Complexed with an RNA/DNA Hybrid: Insight into HIV Reverse Transcription. Molecular Cell. 2007; 28:264–276. [PubMed: 17964265]

NIH-PA Author Manuscript NIH-PA Author Manuscript NIH-PA Author Manuscript

9. Stein CA, Subasinghe C, Shinozuka K, Cohen JS. Physicochemical properties of phosphorothioate oligodeoxynucleotides. Nucleic Acids Res. 1988; 16:3209–3221. [PubMed: 2836790]
10. Cummins L, Graff D, Beaton G, Marshall WS, Caruthers MH. Biochemical and Physicochemical Properties of Phosphorodithioate DNA. Biochem. 1996; 35:8734–8741. [PubMed: 8679636]
11. Rait VK, Shaw BR. Boranophosphates support the RNase H cleavage of polyribonucleotides. Antisense Nucleic Acid Drug Dev. 1999; 9:53–60. [PubMed: 10192289]
12. Noronha AM, Wilds CJ, Lok CN, Viazovkina K, Arion D, Parniak MA, Damha MJ. Synthesis and Biophysical Properties of Arabinonucleic Acids (ANA): Circular Dichroic Spectra, Melting Temperatures, and Ribonuclease H Susceptibility of ANA,RNA Hybrid Duplexes. Biochem. 2000; 39:7050–7062. [PubMed: 10852702]
13. Wang JX, Sergueev DS, Shaw BR. The Effect of a Single Boranophosphate Substitution with Defined Configuration on the Thermal Stability and Conformation of a DNA Duplex. Nucleosides, Nucleotides, and Nucleic Acids. 2005; 24:951–955.
14. Wang X, Dobrikov M, Sergueev D, Shaw BR. RNase H Activation by Stereoregular Boranophosphate Oligonucleotide. Nucleos Nucleot Nucl. 2003; 22:1151–1153.
15. Li P, Sergueeva ZA, Dobrikov M, Shaw BR. Nucleoside and oligonucleoside boranophosphates: chemistry and properties. Chem Rev. 2007; 107:4746–4796. [PubMed: 17967037]
16. Koziolkiewicz M, Krakowlak A, Kwinkowski M, Boczkowska M, Stec WJ. Stereodifferentiation the effect of P chirality of oligo(nucleoside phosphorothioates) on the activity of bacterial RNase H. Nucleic Acids Res. 1995; 23:5000–5005. [PubMed: 8559657]
17. Naoki I, Natsuhisa O, Takeshi W. Stereocontrolled synthesis of oligodeoxyribonucleoside boranophosphates via stereodefined H-phosphonate intermediates. Nucleic Acids Symposium Series. 2009; 53:9–10. [PubMed: 19749234]
18. Anup S, Shaw BR, Spielvogel BF. Boron-Containing Nucleic Acids 2.[1] Synthesis of Oligodeoxynucleoside Boranophosphates. J Am Chem Soc. 1990; 112:9000–9001.
19. Shaw BR, Madison J, Sood A, Spielvogel BF. Oligonucleoside boranophosphates (borane phosphonate). Methods in Mol Biol. 1993; 20:225–243. [PubMed: 8242139]
20. Li H, Huang F, Shaw BR. Conformational Studies of Dithymidine Boranomonophosphate Diastereoisomers. Bio Organic Med Chem. 1997; 5:787–795.
21. Aramini JM, Germann MW. Solution Structure of a DNA RNA Hybrid Containing an a Anomeric Thymidine and Polarity Reversals: d(ATTGG-3′-3′-aT-5′-5′-GCTC) r(gagcaccau). Biochem. 1999; 38:15448–15458. [PubMed: 10569927]
22. Aramini JM, Cleaver SH, Pon RT, Cunningham RP, Germann MW. Solution Structure of a DNA Duplex Containing an a Anomeric Adenosine: Insight into Substrate Recognition by Enodnuclease IV. J Mol Biol. 2004; 338:77–91. [PubMed: 15050824]
23. Sklenár V, Miyashiro H, Zon G, Miles T, Bax A. Assignment of the ^{31}P and ^{1}H resonances in oligonucleotides by two-dimensional NMR spectroscopy. FEBS Lett. 1986; 208:94–98. [PubMed: 3770213]
24. Goddard, TD.; Kneller, DG. SPARKY. Vol. 3. University of California; San Francisco:
25. Bax A, Tjandra N, Zhengrong W. Measurements of ^{1}H-^{31}P dipolar couplings in a DNA oligonucleotide by constant time NOESY difference spectroscopy. J Mol Biol. 2001; 19:367–270.
26. Case, DA.; Darden, TA.; Cheatham, TE., III; Simmerling, CL.; Wang, J.; Duke, RE.; Luo, R.; Merz, KM.; Pearlman, DA.; Crowley, M.; Walker, RC.; Zhang, W.; Wang, B.; Hayik, S.; Roitberg, A.; Seabra, G.; Wong, KF.; Paesani, F.; Wu, X.; Brozell, S.; Tsui, V.; Gohlke, H.; Yang, L.; Tan, C.; Mongan, J.; Hornak, V.; Cui, G.; Beroza, P.; Mathews, DH.; Schafmeister, C.; Ross, WS.; Kollman, PA. AMBER. Vol. 9. University of California; San Francisco: 2006.
27. Summers JS, Roe D, Boyle PD, Colvin M, Shaw BR. Structural Studies of a Borane-Modified Phosphate Diester Linkage: Ab Initio Calculations on the Dimethylboranophsphate Anion and the Single-Crystal X-ray Structure of Its Diisopropylammonium Salt. Inorg Chem. 1998; 37:4158–4159. [PubMed: 11670542]
28. Frisch MJ, Trucks GW, Schlegel HB, Scuseria GE, Robb MA, Cheeseman JR, Montgomery JA Jr, Vreven T, Kudin KN, Burant JC, Millam JM, Iyengar SS, Tomasi J, Barone V, Mennucci B, Cossi M, Scalmani G, Rega N, Petersson GA, Nakatsuji H, Hada M, Ehara M, Toyota K, Fukuda R, Hasegawa J, Ishida M, Nakajima T, Honda Y, Kitao O, Nakai H, Klene M, Li X, Knox JE,

NIH-PA Author Manuscript

NIH-PA Author Manuscript

NIH-PA Author Manuscript

Hratchian HP, Cross JB, Bakken V, Adamo C, Jaramillo J, Gomperts R, Stratmann RE, Yazyev O, Austin AJ, Cammi R, Pomelli C, Ochterski JW, Ayala PY, Morokuma K, Voth GA, Salvador P, Dannenberg JJ, VG. Gaussian 03, Revision C.02.

29. Dupradeau F-Y, Pigache A, Zaffran T, Savineau C, Lelong R, Grivel N, Lelong D, Rosanski W, Cieplak P. The R.E.D. tools: Advances in RESP and ESP charge derivation and force field library building. Phys Chem Chem Phys. 2010; 12:7821–7839. [PubMed: 20574571]
29. Pigache, P.; Cieplak, F-Y.; Dupradeau. Automatic and highly reproducible RESP and ESP charge derivation: Application to the development of programs RED and X RED. 227th ACS National Meeting; Anaheim, CA, USA. March 28–April 1; 2004.
30. Keepers JW, James TL. Two-dimensional nuclear overhauser effect spectra. J Magn Reson. 1984; 57:404–426.
30. Borgias BA, James TL. COMATOSE, a method for constrained refinement of macro-molecular structure based on two-dimensional nuclear Overhauser effect spectra. J Magn Reson. 1988; 79:493–512.
30. Thomas PD, Basus VJ, James TL. Protein solution structure determination using distances from two-dimensional nuclear Overhauser effect experiments: effect of approximations on the accuracy of derived structures. Proc Natl Acad Sci USA. 1991; 88:1237–1241. [PubMed: 1996325]
31. Borgias BA, James TL. Two-dimensional nuclear Overhauser effect: complete relaxation matrix analysis. Methods Enzymol. 1989; 176:169–183. [PubMed: 2811685]
31. Borgias BA, James TL. MARDIGRAS: a procedure for matrix analysis of relaxation for discerning geometry of an aqueous structure. J Magn Reson. 1990; 87:475–487.
32. Rinkel LJ, Altona C. Conformational analysis of the deoxyribofuranose ring in DNA by means of sums of proton-proton coupling constants: A graphical method. J Biomol Struct Dyn. 1987; 4:621–649. [PubMed: 2856025]
33. Mujeeb A, Kerwin SM, Kenyon GL. Solution Structure of a Conserved DNA Sequence from the HIV-1 Genome: Restrained Molecular Dynamics Simulation with Distance and Torsion Angle Restraints Derived from Two-Dimensional NMR Spectra. Biochem. 1993; 32:13419–13431. [PubMed: 8257678]
34. Blackburn, GM.; Gait, MJ.; Loakes, D.; Williams, MD. Nucleic Acids in Chemistry and Biology. 3. The Royal Society of Chemistry; Cambridge UK: 2006.
35. Humphrey W, Dalke A, Schulten K. VMD - Visual Molecular Dynamics. J Molec Graphics. 1996; 14:33–38.
36. Lavery, R.; Sklenar, H. Helical Analysis of Irregular Nucleic Acids. Laboratoire de Biochimie Theorique CNRS; Paris, France: 1996. CURVES 5.1.
37. Wüthrich, K. NMR of Proteins and Nuclic Acids. Wiley-Interscience; New York: 1986.
38. Gorenstein DG, Schroeder SA, Fu JM, Metz JT, Roongta V, Jones CR. Assignments of ^{31}P NMR Resonances in Oligodeoxyribonucleotides: Origin of Sequence-Specific Variations in the Deoxyribose Phosphate Backbone Conformation and the ^{31}PChemical Shifts of Double-Helical Nucleic Acids. Biochem. 1998; 27:7223–7237. [PubMed: 3207672]
39. Li P, Sergueeva ZA, Dobrikov M, Shaw BR. Nucleoside and Oligonucleoside Boranophosphates: Chemistry and Properties. Chem Rev. 2007; 107:4746–4796. [PubMed: 17967037]
40. Hantz E, Larue V, Ladam P, Moyec LL, Gouyette C, Dinh TH. Solution conformation of an RNA–DNA hybrid duplex containing a pyrimidine RNA strand and a purine DNA strand. Int J Biol Macromol. 2001; 28:273–284. [PubMed: 11311717]
41. Gewirtz AM. Oligonucleotide Therapeutics: A Step Forward. J Clin Oncol. 2000; 18:1809–1811. [PubMed: 10784620]
42. Coppelli FM, Grandis JR. Oligonucleotides as anticancer agents: from the benchside to the clinic and beyond. Curr Pharm Des. 2005; 11:2825–2840. [PubMed: 16101440]
43. Cerritelli SM, Crouch RJ. Ribonuclease H: the enzymes in eukaryotes. FEBS J. 2009; 276:1495–1505.

NIH-PA Author Manuscript

NIH-PA Author Manuscript

NIH-PA Author Manuscript

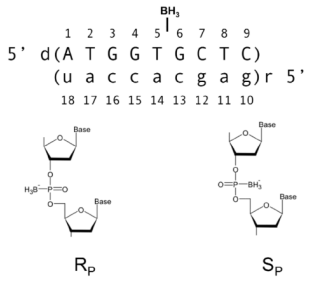

Figure 1.
DNA RNA hybrid design, R_P and S_p denote the chirality of the phosphorus.

NIH-PA Author Manuscript
NIH-PA Author Manuscript
NIH-PA Author Manuscript

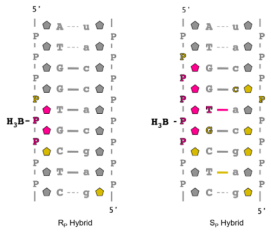

Figure 2.

^{1}H and ^{31}P chemical shift differences at 298K of the R_P and S_P hybrids compared to an unmodified DNA RNA control. ⬟ denotes Σ (|ΔH1′| |ΔH2′1| |ΔH2′2| |ΔH3′|) chemical shifts, **P** phosphorus, **A T G C** |ΔH6| or |ΔH8|. Color scheme as follows: ■ > 0.10 Δ ppm, ■ 0.10–0.05 Δ ppm, ■< 0.05 Δ ppm. **----** denotes imino protons visible at 280K, solid line indicates imino protons observed at 298K.

NIH-PA Author Manuscript

NIH-PA Author Manuscript

NIH-PA Author Manuscript

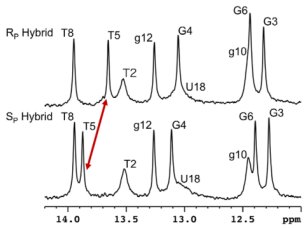

Figure 3.

Imino proton spectra of R_P and S_P hybrids (80 μM duplex, 10 mM sodium phosphate, 100 mM NaCl, 0.1 mM EDTA, 90% H_2O, 280 K, pH 6.2). The red arrow points out the change in the imino proton (T_5) shifts between the two hybrids.

NIH-PA Author Manuscript
NIH-PA Author Manuscript
NIH-PA Author Manuscript

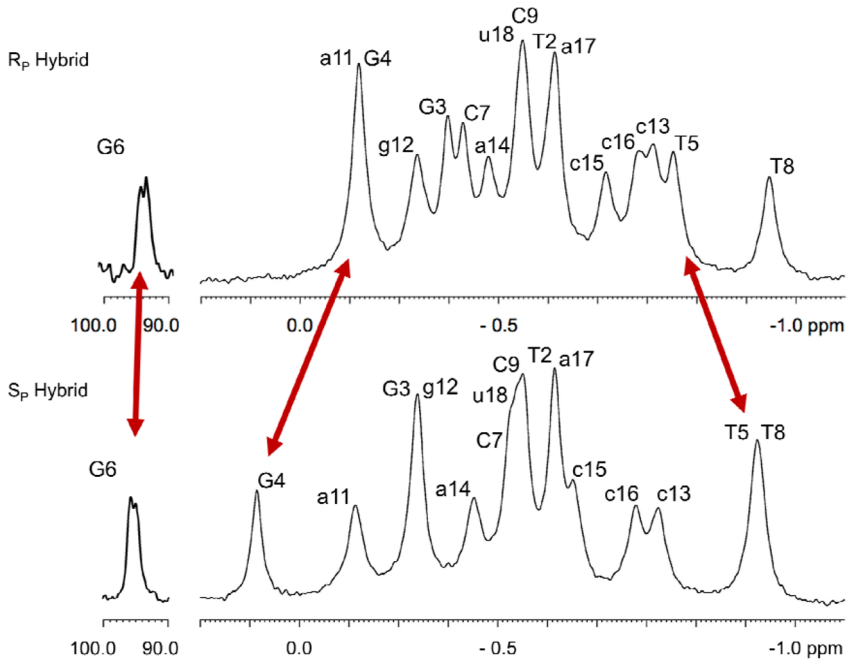

Figure 4.

^{31}P spectra of R_P and S_P hybrids. Assignments were obtained from an HPCOR experiment. Red arrows indicate peaks that have differences > 0.15 ppm between the modified hybrids. The T_5–**P**–G_6 phosphates experiences a large shift (94ppm) due to the BH_3 group, similar to other observed ^{11}B - ^{31}P chemical (39).

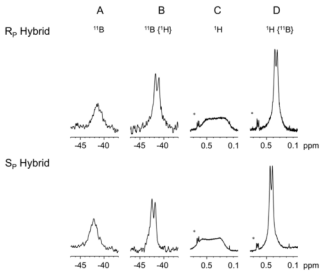

Figure 5.

A) ^{11}B spectra of R_P and S_P hybrids. A single broad peak due to coupling to ^1H and ^{31}P is observed (R_P hybrid −41.43 ppm, S_P hybrid −42.11 ppm). B) Decoupling of ^1H sharpens the ^{11}B peak to a doublet ($^1J_{BP}$ 133 Hz). C) ^1H signal of the BH_3 group, (R hybrid 0.33 ppm, S hybrid 0.42 ppm). D) Decoupling of ^{31}P sharpens the ^1H signal from the BH_3 modification to a doublet. ($^1J_{HB}$ 21.4 Hz) * denotes signal from DSS.

NIH-PA Author Manuscript
NIH-PA Author Manuscript
NIH-PA Author Manuscript

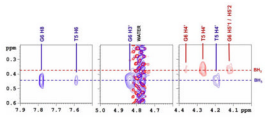

Figure 6.

Boron decoupled {^{11}B} NOESY; the ^{1}H signal from the BH_3 group is sharpened allowing for the detection of cross peaks to nearby sugar (R_P hybrid) and base (S_P hybrid) protons. R_P hybrid contracts show in red, S_P hybrid in blue.

NIH-PA Author Manuscript
NIH-PA Author Manuscript
NIH-PA Author Manuscript

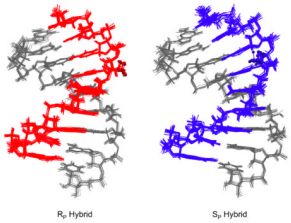

Figure 7.

Aligned (heavy atoms) bundles of the10 final NMR structures. R_P hybrid DNA in red, S_P hybrid DNA in blue, RNA shown in grey. Structures were generated by sampling 1/ps for the final 10ps of a 6.0 ns restrained solvated molecular dynamic simulation (rMD), followed by fully restrained minimization. RMSD of the heavy atoms were, R_P hybrid 0.30 Å, S_P hybrid 0.34 Å.

NIH-PA Author Manuscript
NIH-PA Author Manuscript
NIH-PA Author Manuscript

NIH-PA Author Manuscript

NIH-PA Author Manuscript

NIH-PA Author Manuscript

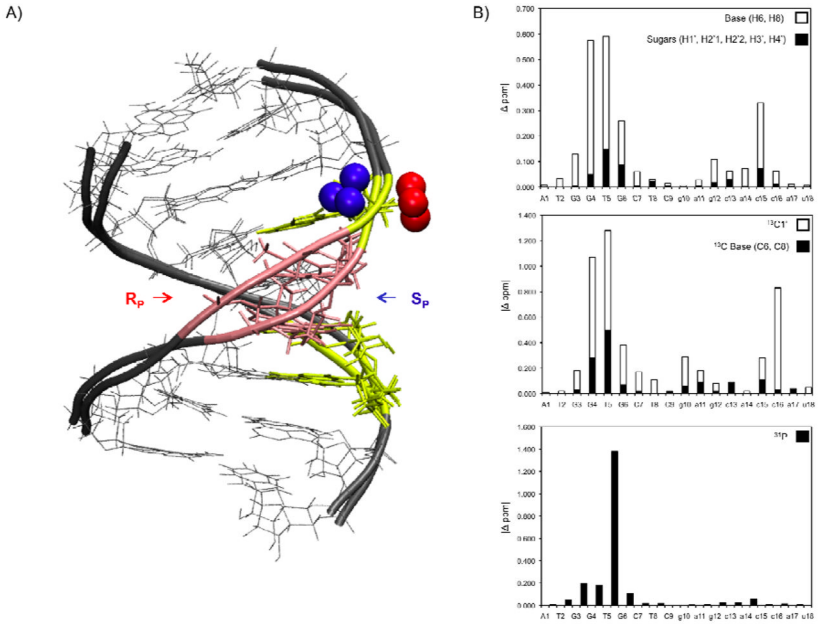

Figure 8.

A) Overlay of R_P and S_P hybrid structures, color coded according to chemical shift differences between the two modified hybrids. R_P and S_P hybrids aligned by all heavy atoms (except boron). Nucleotides (Σ (|H1′| |H2′1| |H2′2| |H3′| |H4′| |H6/H8| |^{13}C1′| |^{13}C6/^{13}C8 |) ■ > 1.00 ppm, 1.00 ppm < ■ > 0.50 ppm, ■ < 0.50 ppm. B) R_P and S_P hybrid chemical shift difference plotted by residue.

^{1}H (top) closed box denotes Σ (|H1′| |H2′1| |H2′2| |H3′| |H4′|), ^{13}C (middle), ^{31}P (bottom) all Δ ppm. T_5–**P**–G_6 (^{31}P) display the largest difference in chemical shift between the two modified hybrids (Δ 1.2 ppm).

NIH-PA Author Manuscript
NIH-PA Author Manuscript
NIH-PA Author Manuscript

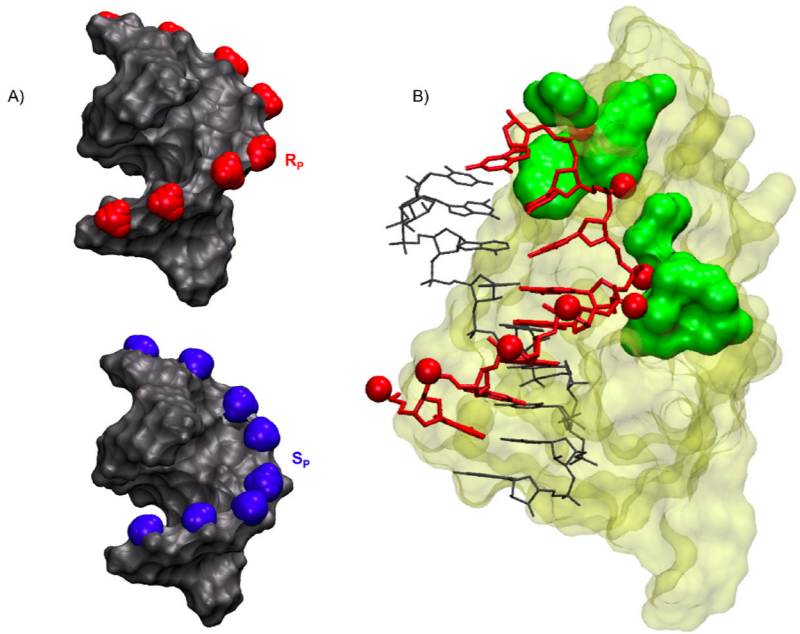

Figure 9.

A) Models of fully stereo specific R_p (red) or S_p (blue) modified BH_3 DNA/RNA hybrids. B) R_p BH_3 modifications (shown as red CPK spheres) were modeled on the existing crystal structure of RNase H1 enzyme (tan) in complex with a DNA (red) RNA (grey) hybrid (8). The enzyme contacts the hybrid along the DNA backbone and in the minor grove (green).

NIH-PA Author Manuscript

NIH-PA Author Manuscript

NIH-PA Author Manuscript

Table 1

Thermodynamic properties of DNA/RNA hybrids containing a central R_p or S_p BH_3 DNA backbone modification and an unmodified control in 10 mM sodium phosphate, 50 mM NaCl, pH 6.4. T_M values were calculated for a 30 μM duplex. ΔG are given for 298 K.

	T_M (K)	ΔH (kJ/mol)	ΔS (kJ/mol K)	ΔG (kJ/mol)
R_p hybrid	313.8 (0.2)	265 (6)	0.747 (0.018)	42.6
S_p hybrid	313.8 (0.2)	263(15)	0.739 (0.043)	42.4
Control[a]	312.9 (0.1)	253 (7)	0.706 (0.022)	42.2

[a] Control sample from previously published work at similar conditions (22).

NIH-PA Author Manuscript

NIH-PA Author Manuscript

NIH-PA Author Manuscript

Table 2

Summary of NMR restraints used for structure development. Qualitative distance restraints were derived using RANDIMARDI procedure similar to previously published methods. (22) Final restrained molecular dynamic simulations (rMD) were run for 6.0 ns solvated in TIP3P water at 300 K with the addition of Na+ ions to neutralize phosphate backbone charges. Final ensembles underwent fully restrained minimization (rEM). 1000 steps steepest decent followed by 1000 steps conjugated gradient RMSD values were measured in VMD 5.21. Final Amber energies were calculated in the absence of H_2O and Na^+ ions.

Parameter	R_P hvbrid	S_p hybrid	Force Constant (k)[a]
Quantitative Distance Restraints (RANDMARDI)			
non exchangeables (total)	194	191	30
intra residue	129	118	30
inter residue (sequential)	56	62	30
inter residue (cross strand)	2	2	30
average well width (Å)	0.47	0.64	
semi - quantitative (weak/medium/strong)	5	5	30
average well width (Å)	2.0	2.0	
exchangeables (total)	10	25	10
Qualitative BH_3 Restraints	2	4	30
Endocyclic Torsion Angle Restraints			
deoxyribose (pseudorotation analysis)	35	30	50
average well width | r2−r3|/N	30	30	
Watson Crick Restraints			
distance	23	23	25
fat angle	23	23	10
Backbone Torsion Angle Restraints			
DNA/RNA hybrid broad restraints	70	70	50
well width α β γ δ ζ (deg)	65, 60, 80, 60	65, 60, 80, 60	
ε (C_T NOESY) (deg)	16	16	k varies 50–200 based on number of data pts
Residual Dipolar Coupling			
total RDC restraints	45	45	1.0 (dwt)
base (C6, C8, C2, C5)	27	27	1.0 (dwt)
sugar (C1′)	18	18	1.0 (dwt)
Total Restraints	405	427	
total restraints/residue	22.3	23.7	
CORMA R^x Values			
T_M (ms)	**R^x intra, R^x inter, R^x total**	**R^x intra, R^x inter, R^x total**	
50	n/a	0.057, 0.060. 0.058	
150	0.048, 0.050, 0.049	0.060, 0.058, 0.059	
250	0.049, 0.065, 0.055	0.055, 0058, 0.056	
Final Amber Parameters			
Total Distance Penalty (kcal/mol)	103.9	51.5	

NIH-PA Author Manuscript

NIH-PA Author Manuscript

NIH-PA Author Manuscript

Parameter	R_p hvbrid	S_p hybrid	Force Constant (k)[a]
Total Angle Penalty (kcal)/(mol)	0.5	0.1	
Total Torsion Angle Penalty (kcal)/(mol)	3.4	0.8	
Residual Dipolar Coupling (RDC) Alignment Constraint (kcal/mole)	7.5	5.3	
Amber Energy[a] (kcal/mol)	−210.0	−138.1	
Bundle of 10 Final Structures			
RMSD of Heavy Atoms	0.30	0.34	

[a](kcal/mol * unit of violation)

NIH-PA Author Manuscript NIH-PA Author Manuscript NIH-PA Author Manuscript

Table 3

Selected helicoidal parameters for the R_P and S_P hybrid. Helical parameters indicate the final NMR structures are similar to an unmodified DNA/RNA hybrid with helical properties in between those of A and B type helixes.

Modified Hybrid Base Pair	Xdisp		Incline		Rise		Twist	
	R_p	S_p	R_p	S_p	R_p	S_p	R_p	S_p
A-U	−3.1	−3.3	8.8	4.6				
T-A	−3.0	−3.0	13.3	7.4	2.6	2.8	21.8	21.6
G-C	−3.4	−3.4	15.8	11.5	3.0	3.5	39.3	42.8
G-C	−3.3	−3.5	16.0	12.2	2.8	3.0	34.9	36.6
T-A	−3.5	−3.1	18.3	8.9	3.0	2.7	33.7	28.5
G-C	−3.2	−3.0	14.3	7.3	2.9	2.8	37.8	35.0
C-G	−3.3	−3.1	13.8	5.7	2.9	2.8	31.5	28.6
T-A	−3.5	−3.3	15.2	7.1	3.1	3.0	35.8	31.7
C-G	−3.2	−3.0	15.0	8.3	3.1	3.0	35.8	36.9
average	**−3.3**	**−3.2**	**14.5**	**8.1**	**2.9**	**3.0**	**33.8**	**32.7**
A DNA	−4.1		12		2.9		32.7	
B DNA	0.8		2.4		3.4		36	
DNA/RNA Hybrids								
Hantz, *et. al*. 2001	−3.3 +/−0.7		10 +/−5		3.1 +/−0.2		33 +/−3	
Aramini, *et. al.* 1999	−3.4 +/−0.2		10+/−2.5		3.0 +/−0.3		32 +/−2	